XL CILAMCE
IBERO-LATIN AMERICAN CONGRESS ON COMPUTATIONAL METHODS IN ENGINEERING
NOVEMBER 11-14, 2019
Praiamar Natal Hotel & Convention
Natal, RN-BRAZIL

CONCENTRATED NUMERICAL APPROACH FOR SIMULATION OF STEEL-CONCRETE COMPOSITE BEAMS WITH PARTIAL SHEAR CONNECTION

Ígor J. M. Lemes
Tawany A. Carvalho
igor.lemes@ufla.br
tawanyacarvalho@gmail.com
Departamento de Engenharia, Universidade Federal de Lavras
Campus Universitário, Lavras, 37200-000, Minas Gerais, Brasil
Luís E. S. Dias
Ricardo A. M. Silveira
Amilton R. Silva
luis_civil12@yahoo.com.br
ricardo@em.ufop.br
amilton@em.ufop.br
Departamento de Engenharia Civil, Universidade Federal de Ouro Preto
Campus Morro do Cruzeiro, Ouro Preto ,35400-000, Minas Gerais, Brasil

Abstract. The present work aims at the implementation and validation of a two-dimensional displacement-based numerical formulation for nonlinear analysis of steel-concrete composite beams with deformable shear connection. A finite element corrotational formulation is adopted in order to allow large displacements and rotations in the numerical model. The degradation of the axial and flexural stiffness is determined exclusively at the nodal points of the structural discretization, characterizing the concentrated plasticity. In the cross sections level, the Strain Compatibility Method is used to capture the axial strains in the component members of the section as well as the slipping at the steel-concrete interface. Thus, the constitutive models of materials under normal stresses and shear connection elements are described by continuous functions. For validation of the proposed numerical formulation, the results obtained are compared with numerical and experimental data available in the literature. Since the model proposed here is based on the concentrated simulation of nonlinear effects, a finite element refinement study is also performed. The numerical responses obtained in this paper are closed to experimental and numerical data presented in literature.

Keywords: Partial shear connection, Steel-concrete composite beam,; Concentrated plasticity, SCM.

1 Introduction

In addition to geometric an materials nonlinearities, and beam-to-column connections, steel-concrete composite structural elements may also exhibit partial interaction. This effect is understood as nonlinearity in the deformable shear connection at the steel-concrete interface. In this sense, the degree of composite action becomes an important property since it can portray how rigid this connection will be.

Most cases of partial shear connection studies focus on steel-concrete composite beam analysis. Thus, a subject much addressed in the literature is related to the accuracy of structural systems response using Euler-Bernoulli theory [1] or Timoshenko's beam theory [2, 3].

The deformable shear connection approach with finite interface elements stands out in the context of generalizing the problem, steel-concrete composite elements, or in the analysis of multilayer elements. Another relevant factor is the explicit introduction of differents stiffnesses and bearing capacity for longitudinal sliding and vertical separation in the connection [4, 5]. With a different methodology, there are several works in which partial shear connection is considered by introducing degrees of freedom into a finite beam-column element [6, 7].

With a one-dimensional finite element for nonlinear plane analysis of steel-concrete composite beams, Valipour and Bradford [8] presented a force-based formulation, where the finite element presents four degrees of freedom per node. In this work, the interface slip was simulated by explicitly distributing the axial force (at the element level), with a fraction of it absorbed by the steel profile and the other by the concrete slab. Still in the force-based method, Chiorean and Buru [9] proposed a finite element with six degrees of freedom capable of capturing the partial shear connection effect. However, the authors consider the slip at the steel-concrete interface in the local formulation at the integration points along the finite element. The deformation field was considered linear with a discontinuity in the slip plane. It is noteworthy that the formulation proposed in this work allows the use of only one finite element per member and the plasticity was considered in a distributed way. In addition, ABAQUS software was used as a tool for comparison of results.

Chiorean and Buru [9] reported that the use of displacement-based formulations present problems related to locking phenomena. These phenomena are linked to an unrealistic stiffening of the structure, such as the loss of precision in assessing the slip locking effect. Although these factors are taken into account, some authors adopted alternative solutions to the mentioned problems and developed their displacement-based formulations. For example, Battini et al. [10] chose to use the stiffness matrix based on the exact solution of the equations that govern the problem of beams with partial shear connection. Sousa Jr et al. [1] focused their solutions on the degree of displacement interpolation functions used.

The numerical simulation of steel-concrete composite beams with partial shear connection considering nonlinear effects concentrated in nodal points is approached in a few papers [11–13]. In all these works, the numerical simulation of the deformable connection is introduced in the numerical models similarly. The simulation is done using the considerations of the AISC LRFD [14] for composite beams design. Basically, the composite section moment of inertia is reduced by explicitly considering the degree of interaction provided by the shear connectors. It is worth noting that NBR 8800 [15] follows the same procedure. Thus, this field still open to research and improvement in the formulation proposals, considering concentrated plasticity and partial shear connection, being the objective of this work.

2 Finite element formulation

In the present work, the displacement-based formulation with concentrated plasticity in the nodal points is applied. In this case, the axial and flexural stiffness degradation occurs exclusively at the FE nodes. Then, the method is presented, introducing the geometric, material and shear connections nonlinearities.

It is important to highlight some considerations involving the finite element formulation used in this paper:

- All elements are initially straight, prismatic and the cross-section remains plane after deformation;

- the effects of global instability that may occur in three-dimensional problems (e.g., lateral and torsional buckling) are ignored considering a locking system out of plane;
- the effects of local instability are neglected, such effects as the buckling of the steel section plates, so the section can reach its full plastic rotation capacity;
- large displacements and rigid body rotations are allowed;
- the shear strains effects are ignored;
- yielding of the cross-section is governed by only normal stress;
- there is full interaction between concrete slab and steel reinforcement bars;
- there is no vertical separation of the elements in the interface (uplift); and
- the friction between steel and concrete is neglected.

2.1 Kinematics relations

Figure 1 shows the kinematics of the element and the displacements (translations and rotations) notations used below. If the structural element presents large displacements and/or large rotations, the global degrees of freedom contain the rigid motion and the deformational part. The co-rotational approach aims to separate these parts.

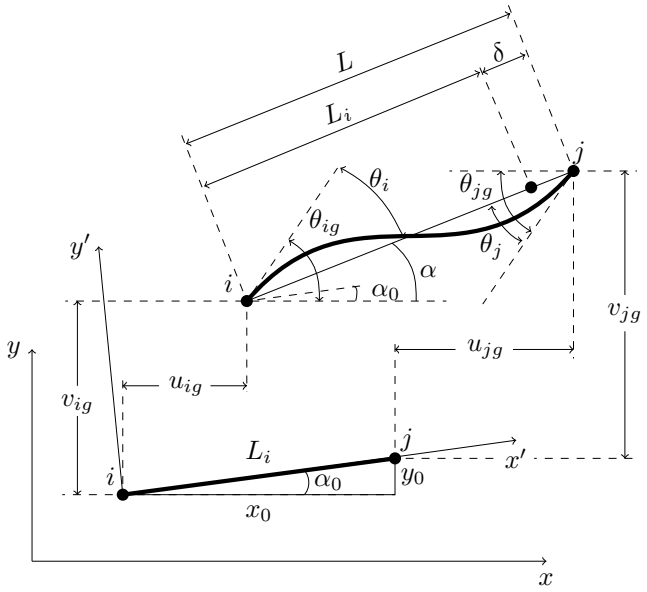

Figure 1. Displacements in global system coordinates

Chhang et al. [16] described the rigid body motion is defined by the global displacements (translations u_{ig} and v_{ig}, and rigid rotation $\alpha - \alpha_0$). It defines a local coordinate system (x', y') that moves continuously with the element. The local system is used to describe the deformational part of the motion.

The relation between global $(u_{ig}, v_{ig}, \theta_{ig}, u_{jg}, v_{jg}, \theta_{jg})$ and local $(\delta, \theta_i, \theta_j)$ degrees of freedom is obtained by a simple differentiation of the co-rotational displacements described in function of global displacements and can be seen in [17]. In a matrix form, this relation is expressed by:

$$\Delta \mathbf{u}_l = \mathbf{B} \Delta \mathbf{u}_g \tag{1}$$

where $\Delta \mathbf{u}_l$ and $\Delta \mathbf{u}_g$ are the incremental displacements in local and global systems, respectively, and the transformation matrix $\mathbf{B}$ is responsible to transform the global displacements in local responses and vice-versa, being:

$$\mathbf{B} = \begin{bmatrix} -c & -s & 0 & c & s & 0 \\ -s/L & c/L & 1 & s/L & -c/L & 0 \\ -s/L & c/L & 0 & s/L & -c/L & 1 \end{bmatrix} \tag{2}$$

in which s is $\sin\alpha$, c is given by $\cos\alpha$ an L is the FE length.

2.2 Element formulation

The corotational approach is convenient for establishing the relationship between the local and global variables [18]. Starting from the Virtual Work Principle, it is possible to describe a relation between the forces in the two referential systems, such as:

$$\Delta V = \Delta \mathbf{u}_g^T \mathbf{f}_g = \Delta \mathbf{u}_l^T \mathbf{f}_l = \Delta \mathbf{u}_g^T \mathbf{B}^T \mathbf{f}_l \tag{3}$$

Using the Eq. (3), the relation between the global, $\mathbf{f}_g$, and local, $\mathbf{f}_l$, forces vector is given by:

$$\mathbf{f}_g = \mathbf{B}^T \mathbf{f}_l \tag{4}$$

By taking the differentiation of Eq. (4) in relation to global displacement vector, $\Delta\mathbf{u}_g$, the global stiffness matrix is described as:

$$\mathbf{K}_g = \frac{\Delta \mathbf{f}_g}{\Delta \mathbf{u}_g} = \mathbf{B}^T \mathbf{K}_l \mathbf{B} + \frac{\mathbf{z}\mathbf{z}^T}{L} N + \frac{1}{L^2}\left(\mathbf{r}\mathbf{z}^T + \mathbf{z}\mathbf{r}^T\right)(M_i + M_j) \tag{5}$$

where $\mathbf{K}_l$, N, M_i and M_j are the stiffness matrix and the forces in local system, respectively, and:

$$\mathbf{r} = \begin{bmatrix} -c & -s & 0 & c & s & 0 \end{bmatrix}^T \tag{6}$$

$$\mathbf{z} = \begin{bmatrix} s & -c & 0 & -s & c & 0 \end{bmatrix}^T \tag{7}$$

2.3 Stiffness matrix in local system

Lower-order interpolation functions are associated with locking phenomena in displacement-based FE formulations. Tang et al. [19] pointed out membrane locking would arise when a straight beam-column element with low-order axial displacement interpolation is used in the geometrical nonlinear analysis. Using the degenerated form of the Green strain and the curvature based on Euler-Bernoulli hypotheses, the normal axial strains are described as:

$$\varepsilon = \frac{du}{dx} + \frac{1}{2}\left(\frac{dv}{dx}\right)^2 \tag{8}$$

$$\Phi = -\frac{d^2 v}{dx^2} \tag{9}$$

Assuming that the total axial displacement can be divided into stretch and flexure-induced displacement, according Tang et al. [19] the transversal (v) and axial (u) displacement interpolations that eliminate the membrane locking are given by:

$$v = x\left(1 - \frac{x}{L}\right)^2 \theta_i + \frac{x^2}{L}\left(\frac{x}{L} - 1\right)\theta_j \tag{10}$$

$$u = \underbrace{\frac{x}{L}\delta}_{\text{stretch}} + \underbrace{\frac{x}{L}\int_0^L \frac{1}{2}\left(\frac{dv}{dx}\right)^2 dx - \int_0^x \frac{1}{2}\left(\frac{dv}{dx}\right)^2 dx}_{\text{flexure}} \tag{11}$$

From Eq. (11), the axial strain as function of nodal displacement and rotations as follows:

$$\varepsilon = \frac{\delta}{L} + \frac{2\theta_i^2 - \theta_i\theta_j + 2\theta_j^2}{30} \tag{12}$$

Assuming here the material elastic behavior and the applied load is conservative and nodal, the system potential energy may be expressed by the strain energy U and external work done W, that is:

$$\Pi = U - W = \frac{1}{2}EA\int_0^L \varepsilon^2 dx + \frac{1}{2}EI\int_0^L \Phi^2 dx - \sum_{i=1}^{3} f_{l,i}u_{l,i} \tag{13}$$

where E is the modulus of elasticity, A and I are cross section geometric properties (area and moment of inertia). Using Eqs. (9) and (12) in Eq. (13) the potential energy is now expressed by the elements degrees of freedom. By the principle of stationary potential energy, the first variation on the function yields the equilibrium equations as [19]:

$$\Delta\Pi = \left(\frac{\partial U}{\partial \mathbf{u}_l} - \mathbf{f}_l\right)\Delta\mathbf{u}_l = 0 \tag{14}$$

being the first variation of strain energy, U, results in the internal forces vector, $\mathbf{f}_l$, that is:

$$\mathbf{f}_l = \frac{\partial U}{\partial \mathbf{u}_l} \tag{15}$$

and the tangent stiffness matrix as the second variation of strain energy, or the first variation of internal forces:

$$\mathbf{K}_l = \frac{\partial^2 U}{\partial \mathbf{u}_l^2} = \frac{\partial \mathbf{f}_l}{\partial \mathbf{u}_l} \tag{16}$$

2.4 Concentrated plasticity approach

In the model of the structural systems using corotational-FE, the beam-column finite element is used, defined by nodes i and j, as shown in Fig. 1. The inelastic flexure terms of the matrix $\mathbf{K}_l$ are obtained by a similar approach proposed by Ziemian and McGuire [20]. In order to avoid any numerical integration in calculating element stiffness matrices during the analysis, the flexure terms are calculated considering the moment-curvature relationship $(M \times \Phi)$ tangent varying linearly along the finite element length to the likely situation of a linear moment gradient [20]. Thus:

$$EI\,(x) = \left[\left(1 - \frac{x}{L}\right)EI_{T,i} + \frac{x}{L}EI_{T,j}\right] \tag{17}$$

where $EI_{t,i}$ and $EI_{t,j}$ are the tangent flexural stiffness, obtained as described in Section 3, in the nodal points i and j, respectively.

The reduced stiffness matrix (flexure terms), is defined using the second derivative of Hermite interpolation functions used in Eq. (10) [21], described in $\mathbf{N}$, that is:

$$\mathbf{k}^* = \int_0^L \mathbf{N}^T EI_T\,(x)\,\mathbf{N}dx \tag{18}$$

in which:

$$\mathbf{N}^T = \left[\frac{2}{L}\left(2 - \frac{3x}{L}\right) \qquad \frac{2}{L}\left(1 - \frac{3x}{L}\right)\right] \tag{19}$$

3 Cross sectional analysis

According to the AISC LRFD [14], the Strain Compatibility Method (SCM) is a Euler-Bernoulli-based approach for the evaluation of compact cross-sections. When under external loads, a structure will gradually deform until it reaches equilibrium. Once the internal forces equal the external forces, the deformation stops. This deformation, at the cross-section level, is studied by SCM [22].

To make an accurate analysis of cross-sectional nonlinear behavior under external loads, a correct description of the materials behavior is required. The steel section material is described by a trilinear constitutive model being possible to consider the material strain hardening effect. The residual stress models are disregarding in this study. The concrete and reinforcing bars are considered using the uniaxial behavior described in Lemes et al. [22].

3.1 Cross sectional degrees of freedom

Two situations are considered here: a bare steel section; and a steel-concrete composite beam with a linear degree of composite action. In both situations, to describe the strain distribution, the cross-section discretization in layers, shown in Figure 2, is very efficient [22, 23]. It is done to capture the axial strain, ε in the plastic centroid (PC) of each layer, and then (through the material constitutive relationships) to obtain the respective stresses, σ_i.

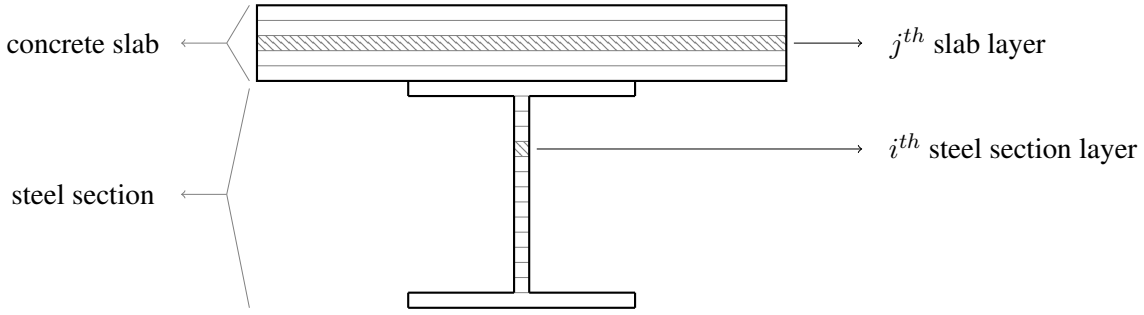

Figure 2. Cross section discretization

In a steel-concrete composite beam section with partial shear connection, the strain field is discontinuous in the steel-concrete interface as showed in Figure 3. Thus, the linear equations that describes the cross sectional deformed shape, in slab ($\varepsilon_{i,slab}$) and steel section ($\varepsilon_{i,steel}$) are expressed as a function of the axial strain in PC of the slab, ε_c, and PC of the steel section, ε_s, respectively. That is:

$$\begin{aligned} \varepsilon_{i,l} &= \varepsilon_c + \Phi\,(y_i - d_{slab}) \\ \varepsilon_{i,p} &= \varepsilon_s + \Phi\,(y_i - d_{steel}) \end{aligned} \tag{20}$$

where d_{slab} and d_{steel} are the distances of the section PC to slab PC and steel section PC, respectively.

In the matrix notation that follows, ε_c, ε_s and Φ are three degrees of freedom of the steel-concrete composite beam section and are components of the strain vector $\mathbf{X}$, described as:

$$\mathbf{X}^T = [\varepsilon_c \quad \varepsilon_s \quad \Phi] \tag{21}$$

Exactly as done previously, the internal force vector for this case is expressed by the classical integration and discretized sums representing the reinforcing bars in concrete slab. Thus:

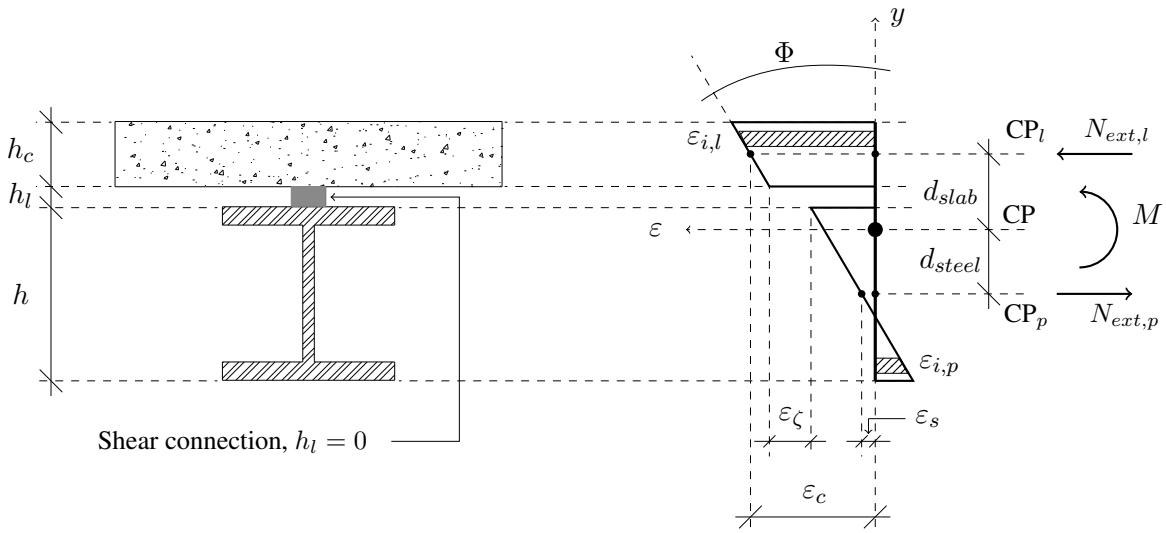

Figure 3. Descontinuous strain field

$$\mathbf{f}_{int} = \left\{ \begin{array}{l} N_{int,slab} = \displaystyle\int_{A_l} \sigma\left[\varepsilon_l\left(\varepsilon_c, \Phi\right)\right] dA + \sum_{i=1}^{n_b} \sigma_i\left[\varepsilon_l\left(\varepsilon_c, \Phi\right)\right] A_{bi} \\ N_{int,steel} = \displaystyle\int_{A_a} \sigma\left[\varepsilon_p\left(\varepsilon_s, \Phi\right)\right] dA \\ M_{int} = \displaystyle\int_{A_l} \sigma\left[\varepsilon_l\left(\varepsilon_c, \Phi\right)\right] y dA + \int_{A_a} \sigma\left[\varepsilon_p\left(\varepsilon_s, \Phi\right)\right] y dA + \sum_{i=1}^{n_b} \sigma_i\left[\varepsilon_l\left(\varepsilon_c, \Phi\right)\right] y_i A_{bi} \end{array} \right\} \tag{22}$$

with A_{ri} being the i^{th} reinforcing bar area and n_b is the number of reinforcing bars. The materials constitutive relationship can be seen in Lemes [17].

In the case of the structural element with partial shear connection, the external axial force is dismembered being part acting on the slab, $N_{ext,slab}$, and another part acting on the steel section, $N_{ext,steel}$. The quantification of the absorbed portions by each component of the cross section is valued considering the possibility of slipping at the steel-concrete interface. Thus, the element external forces, including the total axial force (N) and the external bending moment (M_{ext}), can be writing as:

$$\mathbf{f}_{ext} = \left\{ \begin{array}{c} N_{ext,slab} \\ N_{ext,steel} \\ M_{ext} \end{array} \right\} = \left\{ \begin{array}{c} N_{ext,slab} \\ N - N_{ext,slab} \\ M_{ext} \end{array} \right\} \tag{23}$$

The axial force absorbed by the concrete slab can be defined as a fraction of the portion that would be absorbed if there were full interaction between steel and concrete, N_{slab}^{full} [9]. The reduction factor is defined by $f\left(\gamma_{eff}\right)$, described as a function of the degree of composite action, γ_{eff}. So the axial force on the slab considering deformable shear connection is:

$$N_{ext,slab} = f\left(\gamma_{eff}\right) N_{slab}^{full} \tag{24}$$

The function of degree of composite action, $f\left(\gamma_{eff}\right)$, is discussed below.

3.2 Moment-curvature relation

In describing the strain distribution, the cross section discretization in the layers section, shown in Fig. 2 is very efficient. It is done to capture the axial strain, , in the center of each fiber, and then (through

the material constitutive relations) to obtain the respective stresses, . Thus, the axial strain in i^{th} layer can be obtained as discussed in Subsection 3.1 of this paper.

The cross sectional deformed shape is calculated by the equilibrium of the external, $\mathbf{f}_{ext}$, and internal, $\mathbf{f}_{int}$, forces that can be numerically expressed by the following nonlinear equation:

$$\mathbf{F}(\mathbf{X}) = \mathbf{f}_{ext} - \mathbf{f}_{int} \cong 0 \tag{25}$$

with **F** and **X** being the equilibrium force vector and strain vector, respectively. All of this parameters are dependent of the number of degrees of freedom of the section, as discussed in 3.1. Applying the expansion in Taylor series in Equation 25, results in the following set of nonlinear equations:

$$\mathbf{F}(\mathbf{X}) = \mathbf{F'}(\mathbf{X})\Delta\mathbf{X} \tag{26}$$

where **F'** is the Jacobian matrix of the nonlinear problem, that is:

$$\mathbf{F'}(\mathbf{X}) = -\frac{\partial \mathbf{F}(\mathbf{X})}{\partial \mathbf{X}} \tag{27}$$

Although it is efficient to start the process with **X = 0** , convergence is achieved only in the first iteration if external forces are null. Thus, for the next iteration $(k+1)$, the strain vector is calculated by the Newton-Raphson method as:

$$\mathbf{X}^{k+1} = \mathbf{X}^{k} - \left[\frac{\partial \mathbf{F}(\mathbf{X})}{\partial \mathbf{X}}\right]^{-1} \mathbf{F}(\mathbf{X}^{k}) \tag{28}$$

The iterative process described in this section for a given external forces is illustrated in Figure 4.

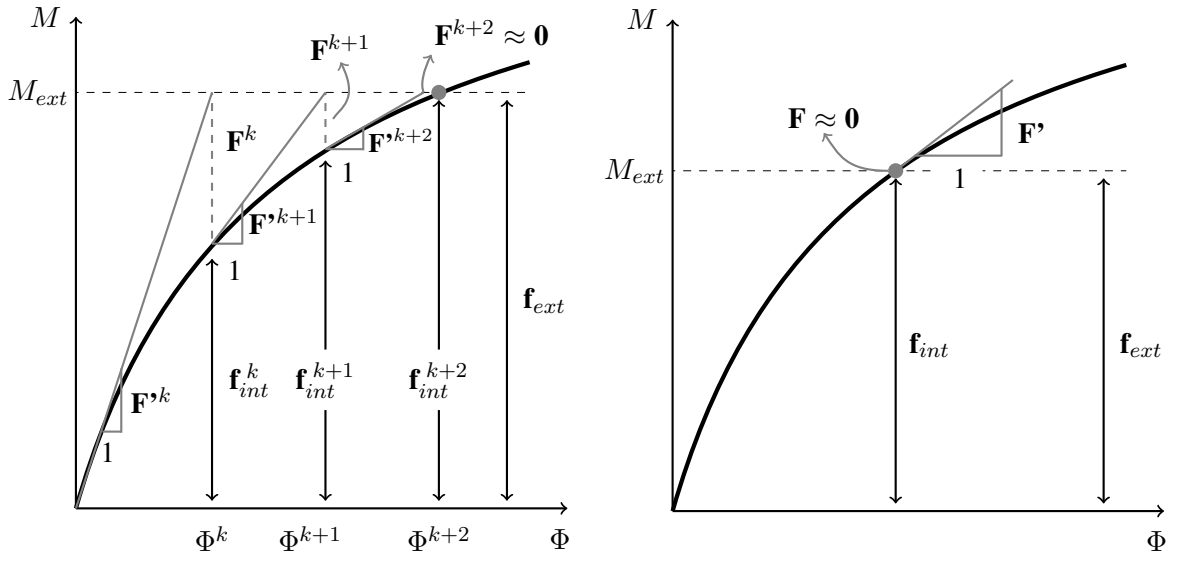

(a) Iterative process (b) Equilibrium point

Figure 4. Moment-curvature relationship

3.3 Generalized stiffness parameters

In the set of equations form, the Equation 26, can be defined as follows:

$$\left\{ \begin{array}{c} \Delta N_{slab} \\ \Delta N_{steel} \\ \Delta M \end{array} \right\} = \left[\begin{array}{ccc} \dfrac{\partial N_{int,slab}}{\partial \varepsilon_c} & \dfrac{\partial N_{int,slab}}{\partial \varepsilon_s} & \dfrac{\partial N_{int,slab}}{\partial \Phi} \\ \dfrac{\partial N_{int,steel}}{\partial \varepsilon_c} & \dfrac{\partial N_{int,steel}}{\partial \varepsilon_s} & \dfrac{\partial N_{int,steel}}{\partial \Phi} \\ \dfrac{\partial M_{int}}{\partial \varepsilon_c} & \dfrac{\partial M_{int}}{\partial \varepsilon_s} & \dfrac{\partial M_{int}}{\partial \Phi} \end{array} \right] \left\{ \begin{array}{c} \Delta \varepsilon_c \\ \Delta \varepsilon_s \\ \Delta \Phi \end{array} \right\} \tag{29}$$

In the steel-concrete composite beam section with partial shear connection, the axial stiffness is calculated by the sum of the slab (EA_{slab}) and steel section (EA_{steel}) axial stiffnesses, such as:

$$EA_T = EA_{slab} + EA_{steel} \tag{30}$$

being:

$$EA_{slab} = \left. \frac{\Delta N_{slab}}{\Delta \varepsilon_c} \right|_{\Delta M=0} \quad ; \quad EA_{steel} = \left. \frac{\Delta N_{steel}}{\Delta \varepsilon_s} \right|_{\Delta M=0} \tag{31}$$

The effective flexural stiffness of the section, EI_{eff}, is expressed as an explicitly dependent of the function of the degree of composite action [9, 17]. Thus:

$$EI_{eff} = \frac{EI_T^{null}}{1 - f\left(\gamma_{eff}\right) \left(\dfrac{EI_T^{full} - EI_T^{null}}{EI_T^{full}} \right)} \tag{32}$$

3.4 Function of degree of composite action

Starting from the studies of Girhammar and Pan [24], Chiorean and Buru [9] and Lemes [17], the function of degree of composite action, $f\left(\gamma_{eff}\right)$, is given by:

$$f\left(\gamma_{eff}\right) = \frac{1}{1 + \left(\pi^2 / \gamma_{eff}\right)} \tag{33}$$

being the degree of composite action, γ_{eff}, is described by [9, 17]:

$$\gamma_{eff} = \mu L \alpha \tag{34}$$

in which μL is the structural element buckling length, α was developed by Girhammar and Pan [24] for an elastic formulation to partial shear connections in composite beams. Thus, Lemes [17] modified this proposal including in a material nonlinear context, ie:

$$\alpha = \sqrt{\frac{k_{Tc} EI_T^{full}}{EA_T^* EI_T^{null}}} \tag{35}$$

where EI_T^{full} and EI_T^{null} are the tangent flexural stiffness of the steel-concrete composite beam with full interaction and null interaction, respectively; EA_T^* is the composite section axial flexural stiffness considering the axial stiffness relation of the concrete slab and steel section in series; k_{Tc} is the connectors tangent stiffness.

3.5 Bending moment capacity

The ultimate bending moment capacity is obtained before the structural analysis (out of incremental-iterative cycle, discussed in Lemes [17] and Lemes et al. [23]. This strategy is adopted to reduce the execution time of the numerical simulations. Thus, the procedure described in Subsection 3.2 is made for each increment of bending moment until it singularizes the Jacobian matrix (Eq. 22). Herein, the incremental strategy is given by [25]:

$$M_{j+1} = M_j + \Phi EI \tag{36}$$

in which the index j refers to the previous increment, Φ is a constant curvature increment, EI is the cross-section flexural stiffness.

The numerical procedure is described in Table 1.

Table 1. Numerical strategy to obtain the ultimate bending moment of the cross section

1.	Read cross-section data and materials
2.	Cross section discretization
3.	Obtain the PC plastic centroid (PC)
4.	Translate the reference system to the (PC)
5.	First value of normal force: $N = 0$
6.	Initialize: $\mathbf{X} = \mathbf{0}$
7.	**for** each increment of bending moment, M, (Equation 36) **do**
8.	Assembly $\mathbf{f}_{ext}$
9.	**for** $k \leftarrow 1, nmax$ **do**
10.	Determine ε (Equations 21)
11.	Assembly f_{int} (Equation 22)
12.	Calculate $\mathbf{F}(\mathbf{X})$ (Equation 25)
13.	**if** $\|\|\mathbf{F}\|\| \div \|\|\mathbf{f}_{ext}\|\| \leq Tol$ **do**
14.	Stop the iterative process and proceed to line 22
15.	**end if**
16.	Assembly the tangent stiffness matrix of section $\mathbf{F}^{'}$ (Equation 29)
17.	Check the $\mathbf{F}^{'}$ singularity
18.	**if** $\mathbf{F}^{'}$ is singular **so**
19.	Save M as the ultimate bending moment
20.	Stop process and proceed to line 25
21.	**end if**
22.	Update the strain vector $\mathbf{X}$ (Equation 28)
23.	**end do**
24.	**end do**
25.	**END PROCESS**

4 Connector stiffness and shear force

Shear connections are usually made by stud-bolt connectors. In this paper, this elements will be consider equally positioned with spacing e_S. Figure 5 shows the disposition of n_l connectors row in a steel-concrete composite specific length. This stretch is delimited by the nodes $i-1$ and $i+1$. Here, the shear force acting in connectors inside of the i^{th} node specific length,l_{cod} is evaluate. For this, it is necessary to know the finite elements lengths commons to the analysed i node, ie, L_j and L_{j+1}

Analysing the free-body diagram of the concrete slab inside the i node specific length, as illustrated in Figure 5, the connection shear force H_{con} can be obtained by the relation between the concrete slab axial internal forces, $N_{int,l}$. Thus:

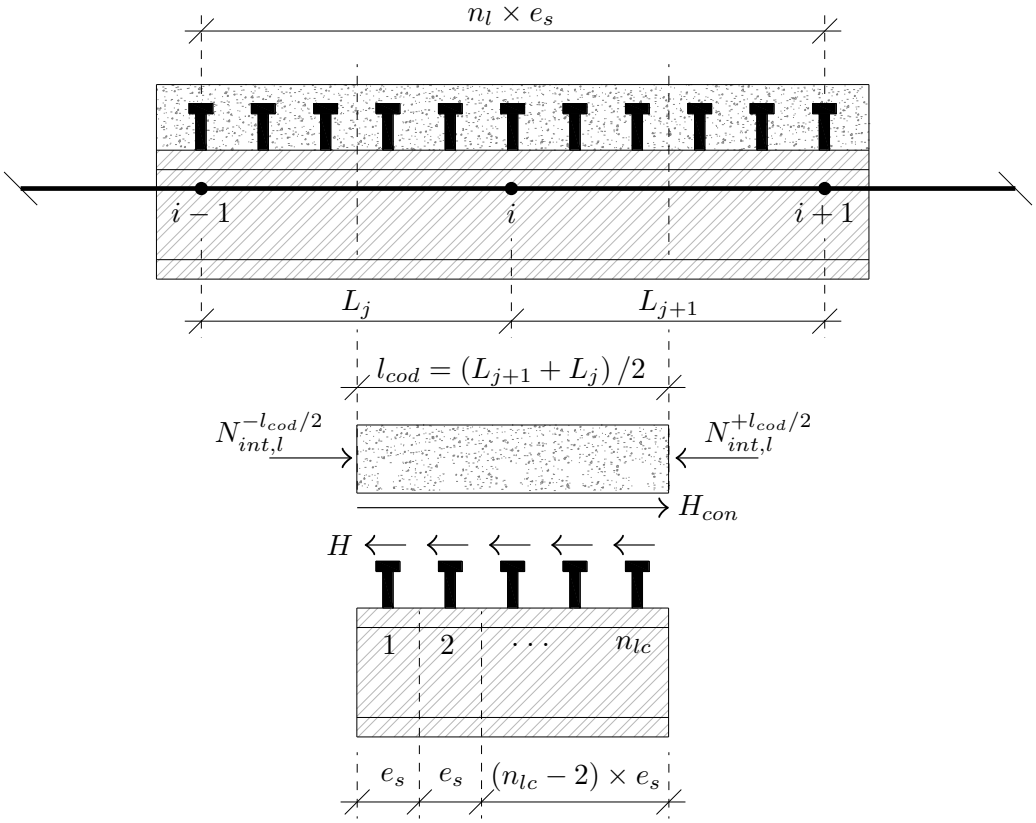

Figure 5. Definition of shear force per length unit in connectors

$$H_{con} = N_{int,l}^{+l_{cod}/2} - N_{int,l}^{-l_{cod}/2} \tag{37}$$

The simplified determination of the shear force in connectors row parallel to cross section plane is made by the following assumption:

$$H = \frac{H_{con}}{n_{lc}} \tag{38}$$

in which n_{lc} is the number of connectors rows in a specific influence length. Thus, if the shear force H is known, the connector stiffness k_{Tc}, relative to spacing, can be obtained by the tangent of Ollgaard et al. [26] constitutive relation.

5 Numerical formulation arrangement

A brief flowchart for the solution of the partial shear connection in steel-concrete composite beams is presented in Table 2. This strategy is applied to obtain the cross section bearing capacity and also to measure the structural element stiffness with deformable connection.

Note that in Table 2 the value of the degree of interaction function is taken to be known. This is because this variable is updated at the end of the global iterative cycle, ie it is kept constant during the iterative process. Thus, once convergence is reached, the parameter α (Equation 35) is calculated at all nodal points present in the beam and consequently $f(\gamma_{eff})$ is updated at each node.

6 Numerical applications

In this section the numerical procedure described in this paper will be tested. The proposed formulation allows for analysis of steel-concrete composite beams with partial shear connection. Hence, some

Table 2. Numerical strategy to obtain the stiffness of element with partial shear connection

1.	Consider $f\,(\gamma_{ef})$, M_{ext}, $N = 0$, section and material data as known
2.	Analyse teh cross section with full interaction to obtain ΔN_l^{tot}
3.	Calculate the axial force in concrete slab, $N_{ext,l}$ (Equation 24)
4.	Assemble the external forces vector (Equation 23)
5.	Initialize: $\mathbf{X} = \mathbf{0}$
6.	**for** k←1, $nmax$ **do**
7.	Determine ε_l and ε_p (Equation 20)
8.	Assemble $\mathbf{f}_{int}$ (Equation 22)
9.	Calculate $\mathbf{F}(\mathbf{X})$ (Equation 25)
10.	**if** $\|\|\mathbf{F}\|\| \div \|\|\mathbf{f}_{ext}\|\| \leq Tol$ **then**
11.	Stop the iterative process and go to line 20
12.	**end if**
13.	Assemble the tangent constitutive section matrix **F'** (Equation 29)
14.	Check the **F'** singularity
15.	**if F'** is singular **then**
16.	Extrapolated ultimate bearing capacity - null stiffness
17.	Stop the process and go to 20
18.	**end if**
19.	Update the strain vector **X** (Equation 28)
20.	**end do**
21.	Calculate the axial end flexural stiffness (Equations 30 and 32)

classic problems in the literature—at both the numerical and experimental levels—will be studied. The examples discussed are divided into two groups: simply supported and continuous beams.

6.1 Simply supported beam

Chapman and Balakrishnan [27] tested simply supported composite beams with partial interaction. In this analysis, the $E1$ beam [27], illustrated in Fig. 6, is simulated using the proposed formulation. In this same figure, loads, geometry, FE meshes and the cross-section are showed. The partial shear connection is made by equally spaced 50 rows with a couple of stud-bolt connectors per row. The material data of this beam are presented in Tab. 3.

Table 3. Material data of simply supported composite beam with partial interaction (in kN, cm)

Material	Data/Value		Material	Data/Value	
Concrete	f_c	3.268	Steel section	f_y	25.82
	ε_{ci}	-0.0022		E_a	20200
	ε_{cu}	-0.00395		E_{a2}	0
Conectors	n_c	100		E_{a3}	350
	n_{cl}	2		ε_u	0.0482
	e_s	12.1	Steel rebar	f_{pyd}	32
	H_{max}	110		E_s	20500

In Tab. 3 there is a only value of f_y for web and flanges of the steel section. However, Chiorean and Buru [9] highlighted the yield stress of the steel section plates are different ($f_{y,flange} = 24.94$ kN/cm^2 and $f_{y,web} = 29.65$ kN/cm^2). To adequate this problem to CS-ASA input, the plastic stress distribution in the steel cross section is made and the full yield bending moment is calculated. Thus, the equivalent yield stress ($f_y = 25.82$ kN/cm^2) is defined by the simple relation between the full yield bending moment and

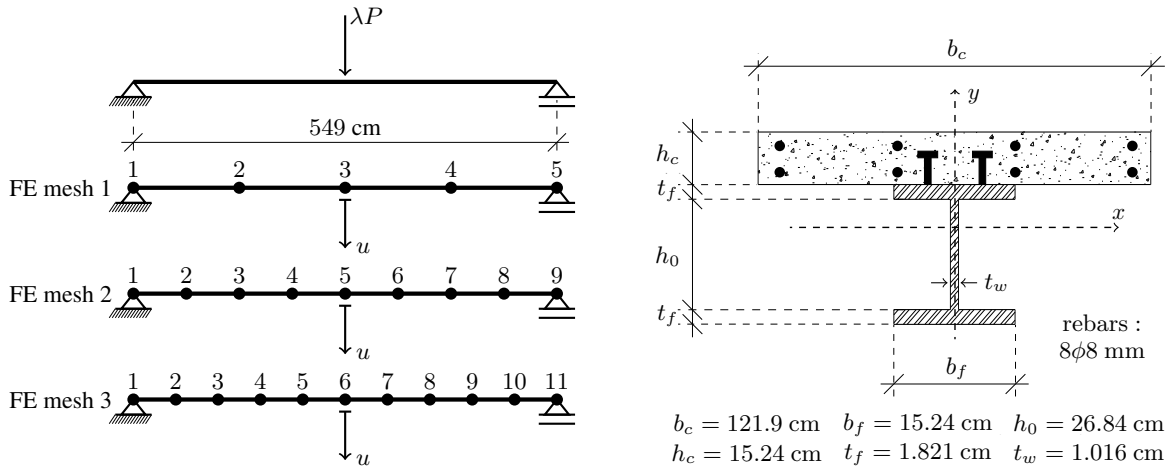

(a) Geometry, loads and adopted FE meshes

(b) Cross section

Figure 6. Simply supported beam with partial shear connection

the plastic section modulus.

In Figure 7 the equilibrium paths for finite element meshes 1,2 and 3 are plotted and compared with the experimental results [27]. As can be seen in this figure, this formulation present a mesh sensibility, the less refined ones being discrepant with respect to the critical load of the structure. This fact is directly related to the concentration of the partial interaction effect at the nodal point. When considering the relative slip between concrete slab and steel section constant within the influence length, l_{cod}, and concentrated at the nodal points, variations of the shear force at the steel-concrete interface in the regions adjacent to the analysed node are disregarded. However, the mesh refinement is sufficient to correct this problem, as can be seen in the FE mesh 3 load-displacement curve. In this mesh, good agreement of the numerical model initial stiffness and critical load can be observed in relation to the experimental results [27].

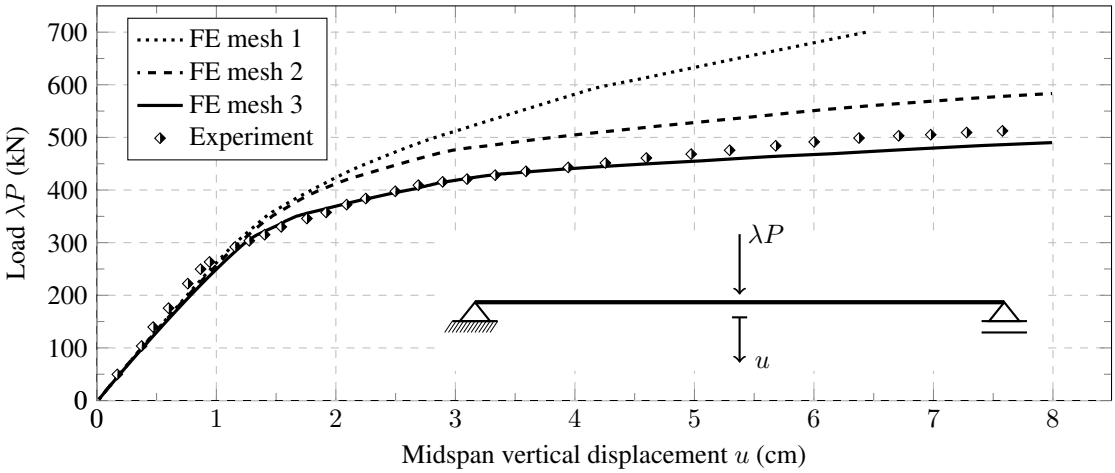

Figure 7. Equilibrium path of simply supported composite beam

6.2 Continuous beams

Unlike previous analysis, here are simulated continuous composite beams with partial interaction. For this, a couple of two-span beams experimental results obtained by Ansourian [28] are used. In Figure 8 are shown the geometry, loads, FE meshes and the cross section in a generalized way. This situation is particularized for the cases of specimens CTB-1 and CTB-4 considering the data presented in Tab. 4. It

is important to highlight the same procedure to obtain an equivalent yield stress is used here.

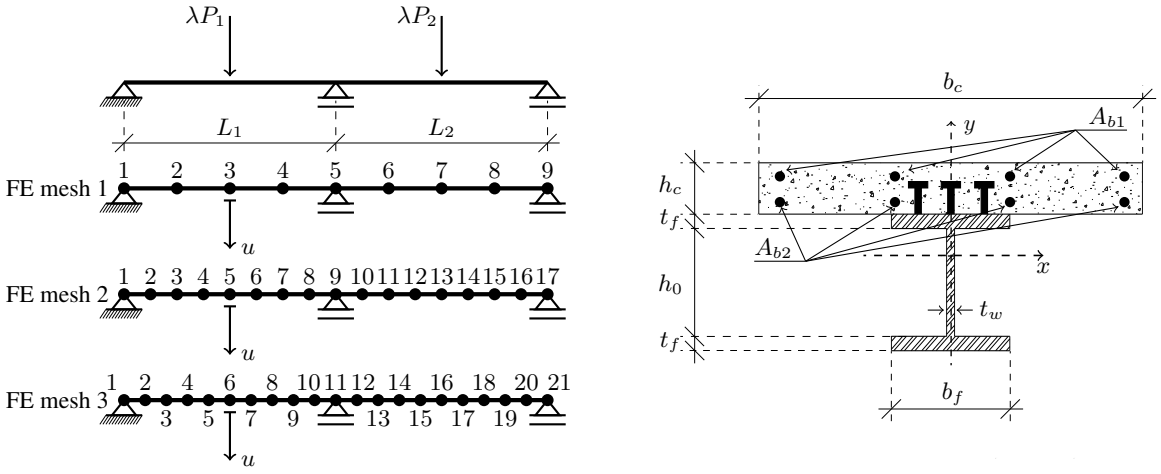

(a) Geometry, loads and adopted FE meshes

(b) Cross section

Figure 8. Continuous composite beams with partial shear connection

The equilibrium paths for these two composite beams with partial interaction are shown in Fig. 9 with experimental results [28]. Although the initial stiffnesses for the three FE meshes are closed to experimental result, the critical load only converge in most refinement meshes. As can be seen in this figure, FE mesh 3 presents good agreement in these two realized simulations allowing the application of the present formulation in the continuous composite beams analysis.

In these three beams, CTB-4 presents different numerical behavior, and convergence was achieved using only FE mesh 3, unlike the CTB-1, where FE mesh 2 already has a good result. Considering the data provided in Tab. 4, it is seen that this beam has a higher number of connectors, implying on the problem already discussed in the previous example. Thus, in order to minimize the variation of the shear force in the steel-concrete interface within the influence length, it is necessary to use a greater number of nodal points, reducing l_{cod}.

7 Conclusions

This paper presented a displacement-based formulation to simulate steel-concrete composite beams wit partial shear connection. The axial force division between the concrete slab and the steel section, in local approach, was sufficient for a close simulation of the actual structural behavior. In this work, it was found that the numerical response considering the effects in a concentrated way approached considerably the experimental responses present in the literature, validating the proposal of the present study. Particular attention has been paid to the study of the finite element mesh, and it is observed that low refinement indices overestimate the connectors stiffness within the influence length, so that the numerical response loses accuracy with respect to the system bearing capacity. This situation has greater visibility as the number of connectors along the structural element length increases. On the other hand, the use of mos refined discretizations is sufficient to correct the problem observed within the context of the formulation presented here. Another form of correction that could be tested is based on the study of the stiffness of the connectors within the influence length, obtaining it more accurately considering the group of connectors as a whole, not just an isolated one.

Acknowledgements

The authors would like to thank CAPES and CNPq (Federal Research Agencies), Fapemig (Minas Gerais State Research Agency), UFOP and UFLA for their support during the development of this work.

Table 4. Geometric and material data of continuous composite beams

Variable and units	Parameter	Beam	
		CTB-1	CTB-4
Load (kN)	λP_1	λP	$0.5\lambda P$
	λP_2	-	$0.5\lambda P$
Length (cm)	L_1	400	450
	L_2	500	450
Rebar area in M^- (cm^2)	A_{b1}	8.00	8.04
	A_{b2}	3.16	7.67
Rebar area in M^+ (cm^2)	A_{b1}	-	1.6
	A_{b2}	1.60	1.60
Slab dimensions (cm)	h_c	10.0	10.0
	b_c	80.0	80.0
Steel section dimensions (cm)	t_f	0.85	1.00
	h_0	18.30	17.00
	b_f	10.00	20.00
	t_w	0.56	0.65
Concrete (kN,cm)	f_c	2.46	2.79
	ε_{ci}	-0.00220	-0.00220
	ε_{cu}	-0.00484	-0.00452
Steel section (kN,cm)	f_y	29.109	23.770
	E_a	20600	20600
	E_{a2}	0	0
	E_{a3}	600	300
	ε_u	0.0287	0.0703
Steel rebar (kN,cm)	f_{pyd}	43	43
	E_s	20600	20600
	E_{s2}	600	300
Connectors (kN,cm)	n_c	66	84
	n_{cl}	2	3
	s	28	33
	H_{max}	110	110

References

[1] Sousa Jr, J. B. M., Oliveira, C. E. M., & Silva, A. R., 2010. Displacement-based nonlinear finite element analysis of composite beam-columns with partial interaction. *Journal of Constructional Steel Research*, vol. 66, pp. 772–779.

[2] Ranzi, G. & Zona, A., 2007. A steel-concrete composite beam model with partial interaction including the shear deformability of the steel component. *Engineering Structures*, vol. 29, pp. 3026–3041.

[3] Nguyen, Q. H., Hjiaj, M., & Lai, V. A., 2014. Force-based FE for large displacement inelastic analysis of two-layer timoshenko beams with interlayer slips. *Finite Elements in Analysis and Design*, vol. 85, pp. 1–10.

[4] Schellekens, J. C. J. & de Borst, R., 1993. On the numerical integration of interface elements. *International Journal for Numerical Methods in Engineering*, vol. 36, pp. 43–66.

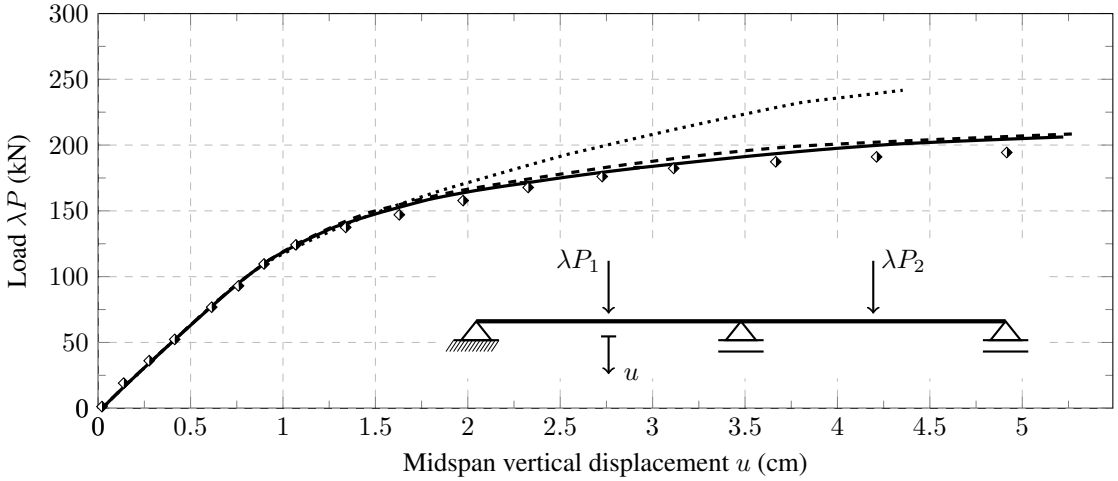

(a) CTB-1

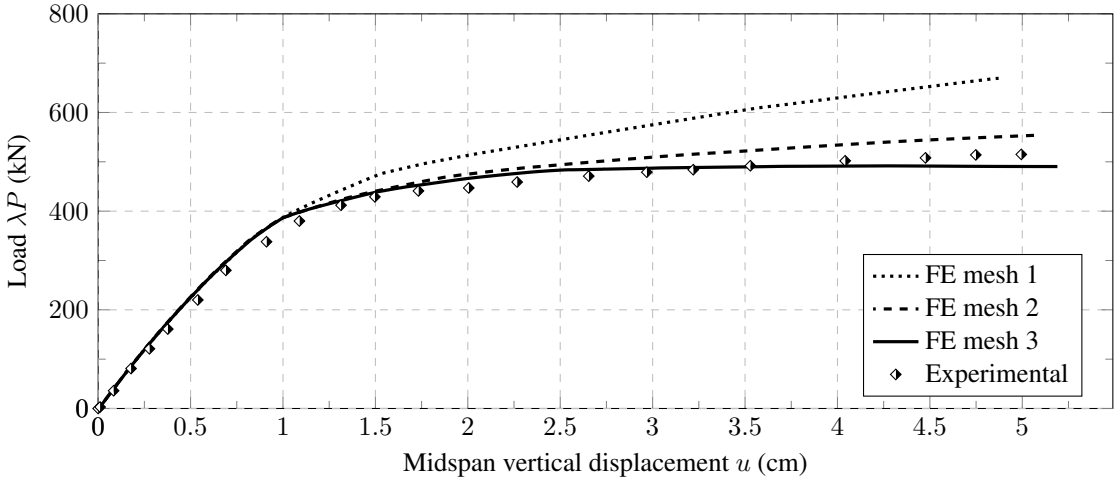

(b) CTB-4

Figure 9. Equilibrium paths for continuous composite beams

[5] da Silva, A. R., 2006. Análise numérica de vigas mistas com interação parcial. Master's thesis, Programa de Pós Graduação em Engenharia Civil, Universidade Federal de Ouro Preto, Ouro Preto, MG, Brasil.

[6] Ayoub, A. & Filippou, F. C., 2000. Mixed formulation of nonlinear steel-concrete composite beam element. *Journal of Structural Engineering*, vol. 126, n. 3, pp. 371–381.

[7] Faella, C., Martinelli, E., & Nigro, E., 2010. Steel-concrete composite beams in partial interaction: closed-form "exact" expression of the stiffness matrix and the vector of equivalent nodal forces. *Engineering Structures*, vol. 32, pp. 2744–2754.

[8] Valipour, H. R. & Bradford, M. A., 2009. A steel-concrete composite beam element with material nonlinearities and partial shear interaction. *Fibre Chemistrynite Elements in Analysis and Design*, vol. 45, pp. 966–972.

[9] Chiorean, C. G. & Buru, S. M., 2017. Practical nonlinear inelastic analysis method of composite steel-concrete beams with partial composite action. *Engineering Structures*, vol. 134, pp. 74–106.

[10] Battini, J. M., Nguyen, Q. H., & Hjiaj, M., 2009. Non-linear finite element analysis of composite beams with interlayer slip. *Computers and Structures*, vol. 87, pp. 904–912.

[11] Liew, J., Chen, H., & Shanmugam, N., 2001. Inelastic analysis of steel frames with composite beams. *Journal of Structural Engineering*, vol. 127, n. 2, pp. 194–202.

[12] Iu, C., Bradford, M., & Chen, W., 2009. Second-order inelastic analysis of composite framed structures based on the refined plastic hinge method. *Engineering Structures*, vol. 31, pp. 799–813.

[13] Iu, C. K., 2016. Nonlinear analysis for the pre and post yield behaviour of a composite structure with the refined plastic hinge method. *Journal of Constructional Steel Research*, vol. 119, pp. 1–16.

[14] AISC LRFD, 2016. Specification for structural steel buildings. *American Institute of Steel Construction, Chicago, IL*.

[15] NBR 8800, 2008. Projeto de estruturas de aço e de estruturas mistas de aço e concreto de edifícios. *Associação Brasileira de Normas Técnicas*.

[16] Chhang, S., Battini, J.-M., & Hjiaj, M., 2017. Energy-momentum method for co-rotational plane beams: A comparative study of shear flexible formulations. *Finite Elements in Analysis and Design*, vol. 134, pp. 41–54.

[17] Lemes, 2018. *Advanced numerical study of steel, concrete and steel-concrete composite structures*. PhD thesis, Federal University of Ouro Preto, Ouro Preto, Brazil.

[18] Alhasawi, A., Heng, P., Hjiaj, M., Guezoulli, S., & Battini, J.-M., 2017. Co-rotational planar beam element with generalized elasto-plastic hinges. *Engineering Structures*, vol. 151, pp. 188–205.

[19] Tang, Y. Q., Zhou, Z. H., & Chan, S. L., 2015. Nonlinear beam-column element under consistent deformation. *International Journal of Structural Stability and Dynamics*, vol. 15, n. 5, pp. 1450068.

[20] Ziemian, R. D. & McGuire, W., 2002. Modified tangent modulus approach, a contributtion to plastic hinge analysis. *Journal of Structural Engineering*, vol. 128, n. 10, pp. 1301–1307.

[21] McGuire, W., Gallagher, R. H., & ZIemian, R., 2000. *Matrix structural analysis*. New York, 2 nd edition.

[22] Lemes, Í. J. M., Silveira, R. A. M., Silva, A. R. D., & Rocha, P. A. S., 2017. Nonlinear analysis of two-dimensional steel, reinforced concrete and composite steel-concrete structures via coupling SCM/RPHM. *Engineering Structures*, vol. 147, pp. 12–26.

[23] Lemes, Í. J. M., Barros, R. C., Silveira, R. A. M., Silva, A. R. D., & Rocha, P. A. S., 2018. Numerical analysis of rc plane structures: a concentrated nonlinear effect approach. *Latin American Journal of Solids and Structures*, vol. 15, n. 2.

[24] Girhammar, U. A. & Pan, D. H., 2007. Exact static analysis of partially composite beams and beam-columns. *International Journal of Mechanical Sciences*, vol. 49, n. 2, pp. 239–255.

[25] Zubydan, A. H., 2013. Inelastic large defletion analysis of space steel frames including H-shaped cross-section members. *Engineering Structures*, vol. 48, pp. 155–165.

[26] Ollgaard, J. G., Slutter, R. G., & Fisher, J. W., 1971. Shear strength of stud connectors in lightweight and normal-weight concrete. *AISC Engineering Journal*, vol. 8, n. 2, pp. 55–64.

[27] Chapman, J. C. & Balakrishnan, S., 1964. Experiments on composite beams. *Structural engineers*, vol. 42, pp. 369–383.

[28] Ansourian, P., 1981. Experiments on continuous comosite beams. *Proceedings of the Institution of Civil Engineer*, vol. 71, n. 2, pp. 25–51.